Color tuning in alert macaque V1 assessed with fMRI and single-unit recording shows a bias toward daylight colors

Rosa Lafer-Sousa,[1,2,†] Yang O. Liu,[1,2,†] Luis Lafer-Sousa,[3] Michael C. Wiest,[1] and Bevil R. Conway[1,2,*]

[1]*Neuroscience Program, Wellesley College, Wellesley, Massachusetts 02481, USA*
[2]*Department of Neurobiology, Harvard Medical School, Boston, Massachusetts 02115, USA*
[3]*Department of Mathematics, Massachusetts Institute of Technology, Cambridge, Massachusetts 02139, USA*
**Corresponding author: bconway@wellesley.edu*

Received September 27, 2011; revised January 27, 2012; accepted January 28, 2012; posted January 31, 2012 (Doc. ID 155222); published April 9, 2012

Colors defined by the two intermediate directions in color space, "orange–cyan" and "lime–magenta," elicit the same spatiotemporal average response from the two cardinal chromatic channels in the lateral geniculate nucleus (LGN). While we found LGN functional magnetic resonance imaging (fMRI) responses to these pairs of colors were statistically indistinguishable, primary visual cortex (V1) fMRI responses were stronger to orange–cyan. Moreover, linear combinations of single-cell responses to cone-isolating stimuli of V1 cone-opponent cells also yielded stronger predicted responses to orange–cyan over lime–magenta, suggesting these neurons underlie the fMRI result. These observations are consistent with the hypothesis that V1 recombines LGN signals into "higher-order" mechanisms tuned to noncardinal color directions. In light of work showing that natural images and daylight samples are biased toward orange–cyan, our findings further suggest that V1 is adapted to daylight. V1, especially double-opponent cells, may function to extract spatial information from color boundaries correlated with scene-structure cues, such as shadows lit by ambient blue sky juxtaposed with surfaces reflecting sunshine.

OCIS codes: 330.1690, 330.1720, 330.4270, 330.4300, 330.5380.

1. INTRODUCTION

Color processing in humans is thought to be mediated by two cardinal chromatic mechanisms that have been characterized psychophysically [1] and that have been accounted for in terms of the physiology of two populations of neurons in the lateral geniculate nucleus (LGN) of macaque monkeys [2]. The two mechanisms have been loosely described as "red–green" and "blue–yellow," although the color terms associated with the colors that yield maximum activation of each mechanism do not align with human color categories of these color names. One chromatic mechanism is characterized by comparing L and M signals (L versus M) and the other by subtracting S from a combination of $L+M$ signals (S versus $L+M$). Together these form the horizontal and vertical (cardinal) axes of the "DKL" color space (Fig. 1A), within which one can also define two intermediate axes: an "orange–cyan" axis and a "lime–magenta" axis. A stimulus comprising lime and magenta colors will have the same spatiotemporal average cone contrast as one comprising orange and cyan colors because both activate the two cardinal mechanisms (channels) to the same extent, but in different phase [3]: both sets of gratings comprise $L-M$ (red–green) and S (blue–yellow) gratings, but the blue phase is paired with the red phase in the lime–magenta gratings and paired with the cyan in the orange–cyan gratings. As we describe in Section 4, the chromaticities of daylight samples taken throughout the day would fall in the same quadrants of DKL space as the orange–cyan intermediate axis (see Fig. 9C below).

An important question of color processing concerns the mechanisms by which LGN signals are subsequently processed by the cerebral cortex to bring about the various dimensions of color including hue, saturation, and brightness, as well as related phenomena like color contrast and color constancy [5]. Functional imaging results in humans show that the responses in primary visual cortex (V1) to the two intermediate axes are not the same magnitude: specifically, the response to colors along the lime–magenta axis is stronger than the response to colors along the orange–cyan axis [3]. That V1 does not respond to the same extent to the two intermediate axes is evidence that V1 plays an important role in transforming the two cardinal axes: the differential response to the two intermediate axes suggests the intermediate axes are recombined in V1 and represented by distinct "higher-order" channels [6].

Here we address the color tuning of V1 with two sets of experiments conducted in alert macaque monkeys. In the first set of experiments, we measure the functional magnetic resonance imaging (fMRI) responses to colors defined by the DKL color space, replicating in macaque monkeys the experiments that Goddard *et al.* [3] conducted in humans; in the second set of experiments, we measure the responses of cone-opponent neurons in V1 of an alert macaque using single-unit recording and analyze the responses in standard DKL color space. As predicted by Goddard *et al.* [3], our fMRI experiments do not show identical responses to the two intermediate axes. But unlike Goddard *et al.* [3], we find a stronger fMRI response to the orange–cyan intermediate axis, not the lime–magenta axis. Our single-unit experiments, which address

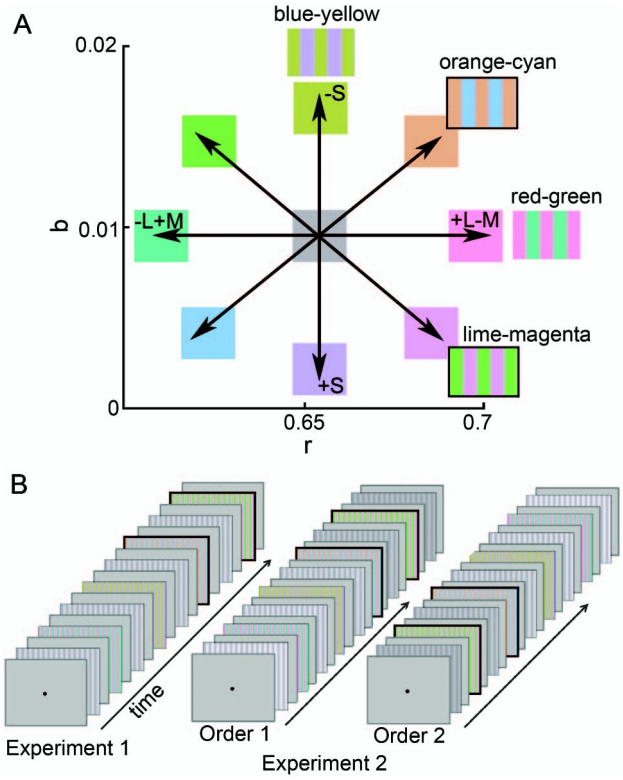

Fig. 1. Experimental design for the fMRI experiments. A. Stimuli were heterochromatic gratings composed of eight colors defined by the isoluminant plane of DKL color space, plotted here in Macleod–Boynton coordinates [2, 4]. Insets show windows from each stimulus condition, with the stimuli of interest to this paper highlighted in black (cyan–orange and lime–magenta). B. Experimental fixation task and fMRI experimental block design. Each frame represents the display presented to the animal. Chromatic stimuli were drifting heterochromatic gratings (2.9 cycles/deg; 0.75 cycle/s) spanning the central 20° of visual field. Two experiments were run, which differed in the sequence of the stimuli and in the contrast of the achromatic gratings (see text for details).

the chromatic tuning of a small subset of V1 neurons, the cone-opponent cells, show a similar bias for orange–cyan.

2. MATERIALS AND METHODS

A. fMRI

Two male rhesus macaques (7–8 kg), M1 and M2, housed in standard 12:12 light–dark cycle and given food *ad libitum* were scanned at Massachusetts General Hospital Martinos Imaging Center (MGH) in a 3-T Allegra (Siemens, New York, New York) scanner using a custom-made four-channel send/receive surface coil (Martinos Center, MGH, Charlestown, Massachusetts) and standard echo planar imaging [repetition time (TR) = 2 s, $98 \times 63 \times 98$ matrix, 1 mm^3 voxels]. Using juice rewards, animals were trained to sit in a sphinx position in a custom-made plastic chair placed inside the bore of the scanner and to fixate a central spot presented on a display screen 49 cm away. Head position was maintained using surgically implanted custom-made plastic head posts (see surgical details below). An infrared eye tracker (ISCAN, Burlington, Massachusetts) was used to monitor eye movements, and animals were only rewarded for maintaining their gaze within ~1° of the central fixation target.

Magnetic resonance (MR) signal contrast was enhanced using a microparticular iron oxide agent (MION), Feraheme (AMAG Pharmaceuticals, Cambridge, Massachusetts), injected intravenously into the femoral vein below the knee just prior to scanning (8–10 mg/kg, diluted in saline). Decreases in MION signals correspond to increases in blood-oxygen-level-dependent (BOLD) response; all MION signals have been inverted to facilitate comparison with BOLD signals.

All imaging and surgical procedures conformed to the local and National Institutes of Health guidelines and were approved by the Harvard Medical School Institutional Animal Care and Use Committee.

B. Surgery

In order to maintain head stabilization during testing, plastic (Delrin) head posts were implanted using standard sterile surgical procedures. Animals were anesthetized with ketamine [15 mg/kg intramuscular (i.m.)] and xylazine (2 mg/kg i.m.) and given atropine (0.05 mg/kg i.m.) to reduce salivary fluid production. Depth of anesthesia was maintained with 1%–2% isoflurane in oxygen administered with a tracheal tube. Animals were given a pre-emptive dose of buprenorphine (0.005 mg/kg i.m.) and flunixin (1.0 mg/kg i.m.) as analgesics and a prophylactic dose of an antibiotic (Baytril, 5 mg/kg i.m.). Antibiotic was administered again 1.5 h into surgery; buprenorphine and flunixin were given for 48 h postoperatively. During the surgery, the animals were placed in a stereotaxic holder, and sterile techniques were used to insert ceramic screws and inverted plastic "T" bolts into the skull. A head post was placed on the surface of the skull and cemented in place to the skull, anchored by the screws and T bolts using dental acrylic. The animals were closely monitored after surgery for signs of pain or infection and treated accordingly. The animals recovered for two months before resuming training.

C. Color Stimuli

For fMRI experiments, visual stimuli were displayed on a screen (41° × 31°) 49 cm in front of the animal using a JVC DLA projector (1024 × 768 pixels). All stimuli spanned the entire screen, contained a small central fixation cross to engage fixation, and were presented in a blocked paradigm.

Color stimuli were generated in DKL color space [2,4] and calibrated using spectral readings taken with a PR-655 spectroradiometer (Photo Research, Inc., Chatsworth, California) using procedures developed by Hansen and Zaidi (personal communication) [7,8]. The spectra were multiplied with the Judd-revised Commission Internationale de l'Eclairage coordinates (CIE) 1931 color matching functions [9,10] to derive CIE xyY coordinates of the monitor phosphors [11]. Eight color directions were chosen, evenly sampling the azimuth of the equiluminant plane of DKL space (Table 1, Fig. 1). Chromaticity coordinates and cone contrasts differed slightly between experiments due to projector bulb performance changing over time. Stimuli were recalibrated one or two days before each experiment.

Color stimuli were presented as heterochromatic vertically oriented trapezoid-wave gratings defined by four chromatic axes [red/green, $+L-M/-L+M$; blue/yellow, $S+/S-$; orange/cyan, $(+L-M)-S/(-L+M)+S$; lime/magenta, $(-L+M)-S/(+L-M)+S$]; the gratings (2.9 cycles/degree, 0.75 cycle/s) were drifted back and forth, switching directions every 2 s [12]. The color names used to describe these stimuli were those used by Goddard *et al.* [3], although these names do not correspond to the names human observers

Table 1. Judd-Corrected CIE *xyY* Values of Stimuli Used in the fMRI Experiments

Experiment 1:	x	y	Y (cd/m^2)
Gray	0.344	0.410	53.13
Red	0.413	0.369	60.03
Orange	0.434	0.450	59.12
Yellow	0.398	0.536	59.59
Lime	0.313	0.546	59.97
Green	0.260	0.467	60.22
Cyan	0.270	0.381	59.06
Blue	0.316	0.337	59.08
Magenta	0.367	0.330	59.62
Black	0.3455	0.4111	46.88
White	0.3449	0.4123	72.69
Experiment 2:	x	y	Y (cd/m^2)
Gray	0.3265	0.4180	117.73
Red	0.3806	0.3845	117.92
Orange	0.3983	0.4616	117.47
Yellow	0.3693	0.5357	118.00
Lime	0.3023	0.5351	117.63
Green	0.2611	0.4593	118.11
Cyan	0.2668	0.3834	117.78
Blue	0.2992	0.3440	117.62
Magenta	0.3420	0.3438	117.91
White 5%	0.3258	0.4179	122.23
Black 5%	0.3260	0.4179	111.87
White 10%	0.3263	0.4191	130.90
Black 10%	0.3264	0.4186	105.38
White 15%	0.3269	0.4185	135.42
Black 15%	0.3263	0.4191	100.69
White 20%	0.3261	0.4189	141.88
Black 20%	0.3267	0.4185	93.63
White 25%	0.3262	0.4186	148.59
Black 25%	0.3263	0.4185	87.87

might use to identify the colors of the gratings. For example, most observers would describe the "orange–cyan" grating as comprising yellowish–orange and blue.

Cone excitation was predicted using the Smith and Pokorny cone fundamentals [13]; lime–magenta and orange–cyan gratings were made so that they generated the same spatio-temporal average Michelson cone contrast (Table 2). Taking lime–magenta as an example, cone contrast (C) was calculated as follows:

$$C_L = (L_{\text{lime}} - L_{\text{magenta}})/(L_{\text{Lime}} + L_{\text{magenta}}),$$
$$C_M = (M_{\text{lime}} - M_{\text{magenta}})/(M_{\text{lime}} + M_{\text{magenta}}),$$
$$C_S = (S_{\text{lime}} - S_{\text{magenta}})/(S_{\text{lime}} + S_{\text{magenta}}),$$

where L_{lime}, M_{lime}, and S_{lime} are the predicted L, M, and S cone activities produced by the lime component of the lime–magenta grating, and L_{magenta}, M_{magenta}, and S_{magenta} are the cone activities produced by the magenta component. Table 2 reports the *absolute value* of the cone contrast for each stimulus. As part of a separate study, we presented achromatic gratings (4%, 10%, 15%, 20%, and 25% luminance contrast) during separate blocks of grating stimulation, although responses to these stimuli are not described here. The present study focuses on responses to the orange–cyan and lime–magenta stimulation periods (blocks) and, in Fig. 5 below, on all the chromatic conditions.

We conducted two fMRI experiments. The first experiment used the four equiluminant chromatic gratings and an achromatic grating of luminance contrast 20% (Fig. 1B, left panel). Blocks in which achromatic or chromatic gratings appeared were separated in time by blocks of uniform gray that were matched in mean luminance to the blocks during which gratings were presented (Table 1). These "gray" blocks allow the fMRI signals to reset to baseline following each grating stimulus. The stimulus sequence of the first experiment consisted of 17 blocks (16 TRs/block, 2 s/TR) in the following order: gray, achromatic grating, gray, red–green grating, gray, achromatic grating, gray, blue–yellow grating, gray, achromatic grating, gray, orange–cyan grating, gray, achromatic grating, gray, lime–magenta grating, and gray. During this experiment, 272 volumes (1 volume/TR) were acquired per scan run (16 volumes/block); each scan run lasted 9 min 4 s.

Table 2. Cone Contrasts of the Stimuli Used in the fMRI Experiments

Experiment 1:	L	M	S
Red–Green	0.065	0.127	0.002
Blue–Yellow	0.010	0.009	0.784
Orange–Cyan	0.047	0.088	0.563
Lime–Magenta	0.045	0.092	0.557
Black–White 20%	0.215	0.217	0.213
Experiment 2:	L	M	S
Red–Green	0.050	0.092	0.001
Blue–Yellow	0.002	0.001	0.707
Orange–Cyan	0.034	0.066	0.501
Lime–Magenta	0.038	0.064	0.502
Black–White 4%	-	-	-
Black–White 10%	0.109	0.109	0.108
Black–White 15%	0.145	0.144	0.144
Black–White 20%	0.205	0.205	0.205
Black–White 25%	0.256	0.256	0.256

The second fMRI experiment used two stimuli sequences (i.e., two orders) and achromatic gratings of various luminance contrasts (Fig. 1B, right panels). Order 1 was gray, achromatic 4%, gray, red–green, gray, achromatic 10%, gray, blue–yellow, gray, achromatic 15%, gray, orange–cyan, gray, achromatic 20%, gray, lime–magenta, gray, achromatic 25%, gray. Order 2 was gray, achromatic 25%, gray, lime–magenta, gray, achromatic 20%, gray, orange–cyan, gray, achromatic 15%, gray, blue–yellow, gray, achromatic 10%, gray, red–green, gray, achromatic 4%, gray. 304 volumes were acquired per scan (16/block), and the scan run lasted 10 min 8 s. Scan runs during which blocks defined by order 1 were interleaved with scan runs of order 2.

D. fMRI Analysis: Region of Interest Definition

Vertically and horizontally oriented achromatic checkered wedges that flickered in phase every 1 s were used to determine the vertical and horizontal meridians of V1 following standard retinotopic mapping techniques (Fig. 2). The stimulus sequence consisted of 32 s of horizontal wedges (99% luminance contrast, occupying 30° visual angle), followed by 32 s of uniform neutral gray, followed by 32 s of vertical wedges (occupying 60° visual angle), followed by 32 s of neutral gray, and so on for a total of four presentations of horizontal wedges and four presentations of vertical wedges. The significance maps comparing fMRI responses to horizontal and vertical wedges were painted on inflated surfaces of each animal's brain and used to define area borders (Fig. 2B).

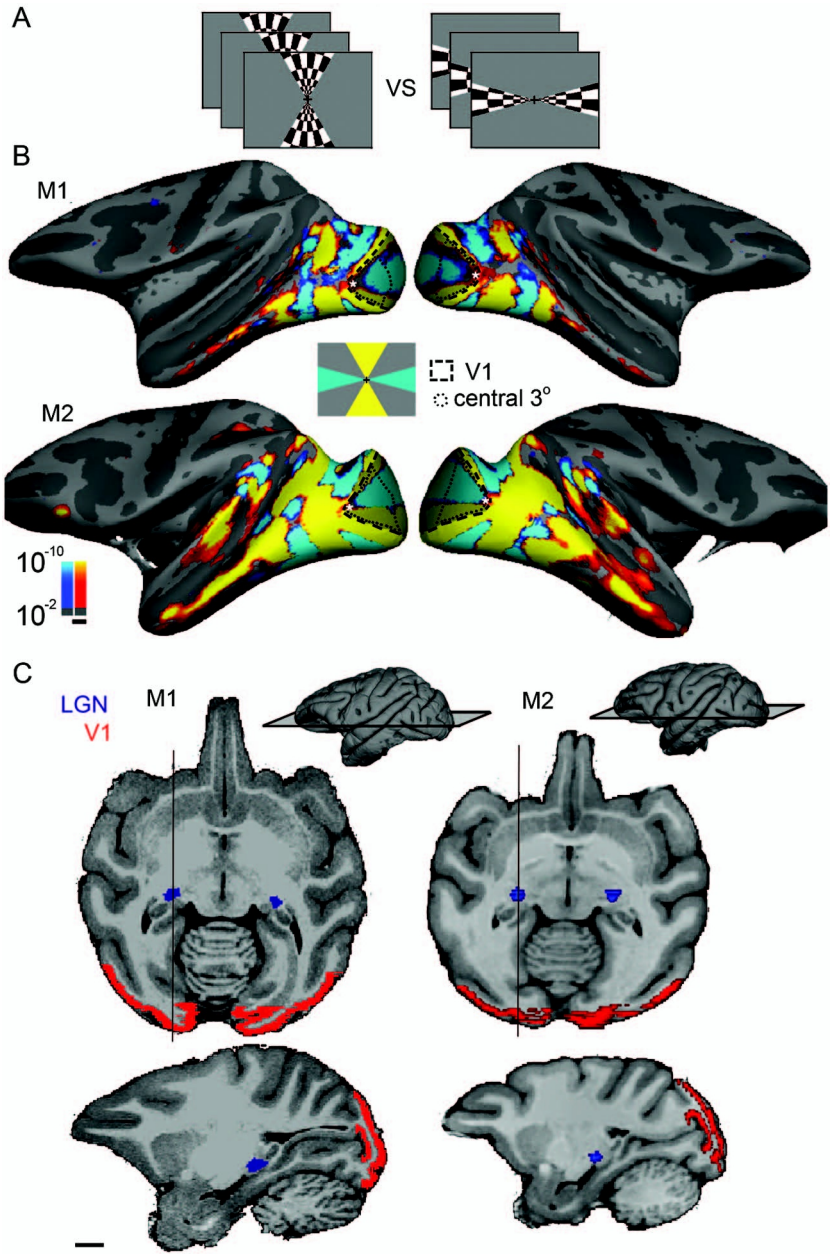

Fig. 2. Identification of ROIs used in fMRI experiments. A. Meridian mapping stimulus used to define retinotopic area boundaries of V1. Vertically (60° wedge) and horizontally (30° wedge) oriented achromatic checkered wedges that flickered in phase every 1 s and spanned the central ~20° of visual field were displayed on a screen 49 cm in front of the animal during recording. The resultant fMRI signals were contrasted to reveal the vertical and horizontal meridians of visual areas. B. Contrast significance maps (horizontal meridians shown in cyan, vertical in yellow) have been painted on inflated volumes, left and right hemispheres for each animal, M1 and M2. The black dashed line marks the boundary of V1. The black dotted line indicates the central 3° visual field representation determined in a separate set of experiments (see Fig. 8); the asterisk represents the fovea. C. ROIs defined for analysis in fMRI experiments shown on high-resolution MR images of each monkey: LGN in blue, V1 in red. Horizontal sections are shown in upper panel; sagittal sections are shown in lower panel. All scale bars indicate 1 cm.

In separate experiments using the same animals, the representation of the central 3° was determined using blocks of flickering achromatic checkerboards that were either restricted to a 3° disc centered on the fixation dot or to the peripheral visual field outside the central 3° (see Fig. 8 below). The dotted contour in Fig. 2B shows the boundary of the representation of the central 3°. In other sessions, high-resolution anatomical scans (0.35 mm × 0.35 mm × 0.35 mm voxels) were obtained for each animal while it was lightly sedated. V1 border assignments were verified by comparing the areal boundaries projected on high-resolution anatomical MRIs of M1 and M2 with standard macaque atlas [14]. V1 regions of interest (ROIs) for each monkey projected on the anatomical MRIs are shown in Fig. 2C (red). ROIs for the LGN were also defined using both functional and anatomical criteria and are shown in Fig. 2C (blue). The numbers of voxels in each ROI are given in Table 3.

E. fMRI Data Processing

A total of 27,344 functional volumes were obtained during four scan sessions in the two macaques. Each scan session consisted of 19–28 stimulus runs (Table 3). The surfaces of the

Table 3. For fMRI Experiments, Number of Voxels in Each Brain Structure and Number of Stimulus Presentations in Each Experiment

ROI/Experiment	M1	M2
# voxels V1, left hemisphere	1331	902
# voxels V1, right hemisphere	1536	817
# voxels, LGN, left hemisphere	39	43
# voxels, LGN, right hemisphere	76	24
# voxels, V1 central 3°, left hemisphere	246	220
# voxels, V1 central 3°, right hemisphere	207	176
# voxels, V1 periphery, left hemisphere	1085	682
# voxels, V1 periphery, right hemisphere	1326	641
# experiment 1 presentations	24	19
# experiment 2 presentations	13	28

high-resolution volumes were reconstructed and inflated; functional data were registered to each animal's own anatomical volume. Data analysis was performed using FreeSurfer software (http://surfer.nmr.mgh.harvard.edu/). Data were motion corrected with the AFNI motion correction algorithm [15] and were intensity normalized. Spatial smoothing was applied to the inflated maps (FWHM = 1.5 mm). More detailed analysis methods are given elsewhere [12,16,17].

Time courses (see Figs. 3 and 5) were calculated by first "detrending" the fMRI response. The temporal drift often associated with fMRI signals was modeled by a second-order polynomial:

$$x(t) = s(t) + at^2 + bt + c,$$

where $x(t)$ was the raw fMRI signal and $s(t)$ was the detrended signal. The coefficients a, b, and c were calculated using the Matlab function *polyfit*. The percentage deviation of the fMRI signal, $s'(t)$, reported as the y-axis values in the time-course traces, was calculated by

$$s'(t) = 100 \times (s(t) - \bar{s})/\bar{s},$$

where $s(t)$, $t = 1, 2, \ldots N$, $\bar{s}$ is the mean of $s(t)$, and N is the number of TRs in the experiment.

To quantify the responses for the bar plots, each voxel's activation in each block was calculated by averaging the response during the last 10 TRs within the block (since each block contained 16 TRs, we calculated the mean of the seventh to the sixteenth samples), subtracting the mean response during the corresponding TRs of preceding and following gray blocks, then dividing by the mean response during the corresponding TRs of the preceding and following gray blocks. Selecting data collected during the last two thirds of each block avoided confounds introduced by the hemodynamic delay and ensured an accurate assessment of the peak fMRI response. Suppose that a block of color stimulus was the kth block in a run. The immediately preceding and immediately following blocks were gray. We denote the response to the stimulus as R^k, which is the mean of the response during the seventh to the sixteenth samples, and the response to the neighboring gray blocks as R^{k-1} and R^{k+1}. The percentage signal change of the stimulus block was then defined by

$$R_S = 100 \times \left(R^k - \frac{R^{k-1} + R^{k+1}}{2}\right) / \left(\frac{R^{k-1} + R^{k+1}}{2}\right).$$

Finally, we restricted our analysis to those voxels with the highest signal-to-noise ratio (SNR). This was done for three

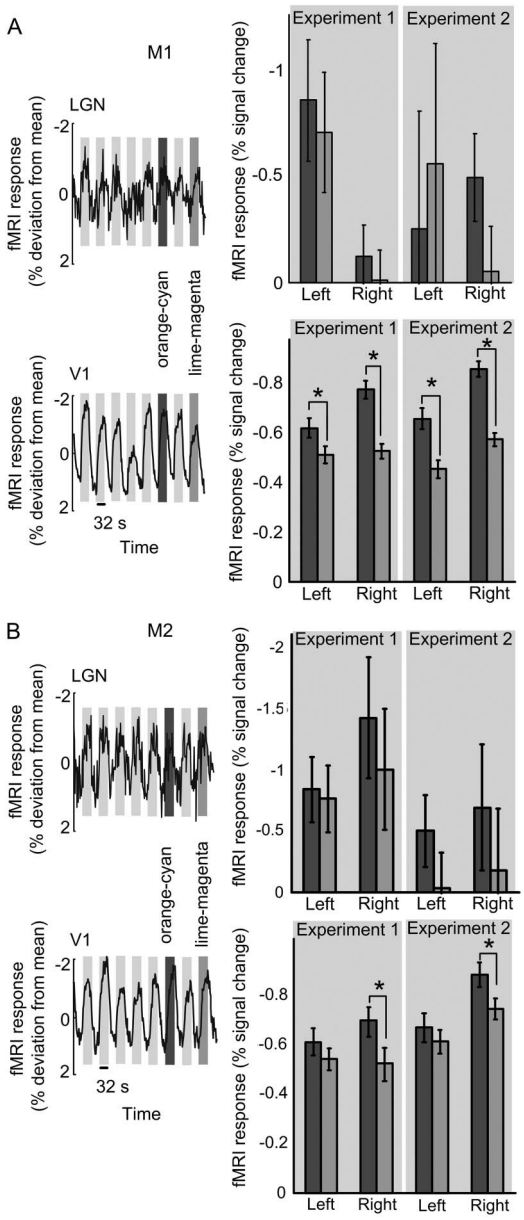

Fig. 3. Macaque V1 shows stronger fMRI responses to orange–cyan over lime–magenta contrasts. A. fMRI results for M1 in LGN and V1. B. fMRI results for M2 in LGN and V1. The left panels show the percentage deviation of the average detrended (second-order polynomial) time courses of response during Experiment 1. Percentage deviation is calculated for each time point as described in Subsection 2.E. For M1, the traces represent the average activity from 24 stimulus presentations ($n = 24$) across 2340 voxels comprising V1 and 97 voxels comprising the LGN. For M2, the traces represent the average activity from 19 stimulus presentations ($n = 19$) across 1404 voxels for V1 and 56 voxels for the LGN. Cyan–orange and lime–magenta responses are highlighted with gray bars. fMRI was conducted using an intravenous MION contrast agent; a decrease in MION signal corresponds to an increase in BOLD. MION signals have been inverted to facilitate comparison with BOLD. Upward deflections in the traces indicate an increase in neural activity. The dips in the traces indicate the baseline response to the neutral-adapting gray. The responses are quantified in the bar plots, which show mean percentage signal changes in each hemisphere ("left," "right") in response to the intermediate colors during Experiments 1 and 2 (the results for Experiment 2 represent the average activity from 13 stimulus presentations ($n = 13$) for M1 and 28 ($n = 28$) for M2; see Table 3 for left- and right-hemisphere ROI voxel numbers). The percent signal change is computed as described in Subsection 2.E. Asterisks represent a significant difference in the magnitude of the response between the conditions ($p < 0.05$, t-test). Error bars indicate 95% confidence intervals.

reasons: first, to account for the possibility of holes in the fMRI signal [18]; second, to remove stray white matter voxels that may have been introduced during the creation of ROIs, which were created manually on the anatomical templates using the functional retinotopic maps for each animal as a guide; third, to mitigate any imperfections introduced by misalignment in the motion correction and template registration steps. The resulting analysis only included voxels of the top 90% SNR assessed during presentation of achromatic grating stimulus blocks (which should drive V1 strongly). A voxel's SNR was calculated by dividing the mean response by the standard deviation.

F. fMRI Classification Analysis

To quantify the extent to which the neural signals recorded from each ROI were capable of discriminating between the orange–cyan and lime–magenta stimuli on the basis of the response to individual presentations of each stimulus, we used a classification algorithm. Following Brouwer and Heeger [19] we used a maximum likelihood classifier, implemented as the Matlab (MathWorks) function *classify* with the option "diaglinear;" the advantage of this algorithm is that it runs relatively quickly. It is, however, unlikely to be optimal for the data here because they may not be normally distributed and noise in neighboring voxels is likely to be correlated rather than independent. As a result, the classifier we used will tend to underestimate the extent to which the two stimuli could be discriminated. Corrections for deviations from normality and correlated noise could improve classification performance [19].

Concretely, the input to the analysis was a matrix of percent-change signal values for the voxels with sufficient signal-to-noise (see Subsection 2.E) with $n$blocks rows and $n$dims columns. $n$blocks indexed the total number of orange–cyan and lime–magenta stimulus presentations included in the analysis. $n\text{dims} = 1$ when we calculated classification performance based on the average signal averaged spatially across voxels and temporally over samples for the univariate classification (see below), and $n\text{dims} = n\text{voxels}$ for the spatial pattern classification (see below). One by one, each row of the data matrix was omitted, and the remaining stimulus blocks were used by the algorithm as a "training set" for extracting regularities in the signal to predict the presence of one or the other stimuli. Then the algorithm was used to attempt to predict which of the two stimuli were presented on the omitted stimulus block—the "testing block." When the algorithm finished attempting to predict the identity of every stimulus block, the result of the "leave-one-out" analysis was the *percent of blocks that were correctly classified*, which provided a simple way to quantify the stimulus-related information available from the signal.

We ran two variants of this analysis. In the univariate analysis, we averaged the signals from samples 7 through 16 of every voxel (ten 2 s samples, the latter two thirds of each block, as described above), such that $n\text{dims} = 1$. This analysis reflects information carried by the overall voxel-averaged and time-averaged signal in each ROI, about the difference between orange–cyan and lime–magenta. In the spatial pattern analysis, the data matrix was averaged over samples 7 through 16 from each voxel in each ROI, but the spatial pattern of activity across voxels was preserved. This analysis could reveal information contained in the spatial pattern of activity across voxels, but conversely, overall classification performance could suffer if many of the voxels carry noisy or irrelevant signals that the algorithm is unable to discount. As described in the results, the pattern analyses rarely revealed any additional information, and so we focus on the univariate analysis. We also ran the above classifications using an alternative algorithm designed to minimize "overfitting," which can occur when the data model involves many parameters. A backpropagation network with fivefold cross validation and 12 hidden units failed to improve univariate or pattern classification as compared to the simple maximum likelihood classifier, suggesting that the classification performances are limited by the data rather than the classification algorithm. The results of this subsequent analysis are not presented.

To quantify the statistical significance of our overall classification results, mean classification performances were compared to each other by a two-tailed t-test or to chance performance of 50% by one-tailed t-test, using the variability over eight recording sessions in two animals.

G. Single-Unit Recording in Alert Macaque V1

The physiological data analyzed in the present report were collected as part of a larger study not involving M1 and M2 [20,21]; detailed experimental methods describing the design of the experiment, the visual stimuli, recording procedures, and data analysis are described in these earlier papers. Here we provide a brief description of the visual stimuli adapted from these papers.

Cone-isolating stimuli were used to evaluate the cone inputs. These stimuli were presented under neutral-adapting conditions produced by a neutral gray background. In any given frame two small colored patches appeared; the location of the patches was confined to a stimulation region about 3° across centered on the receptive field. One of the patches increased a given cone's activity, while the other decreased it (compared to activity elicited in the cones by the neutral-adapting background). Because the cone-isolating stimuli had spatial structure (small patches), the resulting analysis enabled a direct evaluation of the spatial organization of the cone inputs. To generate the stimuli, small patches of the background were replaced with a color that altered the activity of a single cone class at a time using silent substitution. A "+" stimulus increased the activity of the respective cone; a "–" stimulus decreased it. The six cone-isolating stimuli used were as follows (CIE: x, y, luminance in cd/m2): $L+$ (0.413, 0.262, 30.7), $L-$ (0.209, 0.277, 21.3), $M+$ (0.223, 0.336, 28.1), $M-$ (0.378, 0.224, 22.5), $S+$ (0.254, 0.155, 23.1), and $S-$ (0.376, 0.382, 25.9). The adapting background for all experiments was 0.318, 0.271, 25; mean luminance was 25 cd/m2). The cone fundamentals of Stockman and Sharpe [22] were used to estimate cone activity. L and M stimuli were calculated to have equal Michelson's contrast, as follows:

$$[(L+) - (L_{\text{bk}})]/[(L+) + (L_{\text{bk}})] \times 100\%,$$

where $L+$ is the L cone activity produced by the $L+$ stimulus, and L_{bk} is the activity of the L cone produced by the neutral background. The $M+$, $L+$, $M-$, and $L-$ stimuli each had 17% contrast. The $S+$ and $S-$ stimuli each had 41% contrast.

The patches were between 0.25° and 0.75° square; within a given frame, the two patches had no fixed spatial relationship

to each other from one frame to the next. The size of the patches was chosen to be the smallest that still reliably elicited responses. Both patches were the same size and were the same size for all cone stimuli, for a given cell. In any given frame, the two patches could be displayed anywhere relative to each other at 0.06° pixel resolution within a stimulation window between 2.25° and 4.5° square centered on the receptive field. If the patches overlapped, the overlap region appeared as the adapting gray. Enough stimuli were presented so that all locations within the stimulation window were sampled evenly; on average, five presentations were delivered to each pixel location; stimulus runs were on an average 17.5 min per cone map (range of 2–55 min). The same stimulus run (and spike train) was used to generate the response maps for both spots, which was possible because the presentation position of the two spots was independent (the two spots had no consistent spatial relationship from frame to frame). While generating the response map for one of the spots, the activity produced by the other spot was averaged uniformly throughout the map. This average activity, which is common to both + and – maps, is removed during analysis by considering only the difference in activity between the two maps. The stimulus durations were 34–68 ms (two to four frames). The same stimulus duration was used to generate all maps for a given cell. The spatial maps were unaffected by the choice of stimulus duration. From a continuous history of spike timing and stimulus presentation, the average response to each stimulus at each location in the stimulation window was determined; the spatial map at the peak response is given in the present report (see Fig. 9A below).

3. RESULTS

A. V1 Shows a Stronger fMRI Response to Orange–Cyan than Lime–Magenta

Figure 3 shows the mean fMRI response to orange–cyan and lime–magenta stimuli within the LGN and V1 for the two animals tested and the two fMRI experiments that were run (animal "M1" in Fig. 3A; animal "M2" in Fig. 3B). The two fMRI experiments we ran differed in the order in which the stimuli blocks were presented, in the colors that comprised the blocks not analyzed in the present report, and in the magnitude of the cone contrast and mean luminance of the stimuli, as indicated in Tables 1 and 2 and illustrated in Fig. 1. The left panels in Fig. 3 show the time course of the fMRI response from Experiment 1, of each animal's entire V1 and LGN (combining left and right hemispheres). As described below, the right panels (bar plots) in Fig. 3 quantify the responses of the averaged activity from both experiments during the orange–cyan and lime–magenta blocks, for each of the two animal's left and right hemispheres separately. We show the results for the two hemispheres of each animal separately in order to show how reproducible the results are within a given animal's brain. There were no major differences in the results obtained between a given animal's two hemispheres, and results combining both hemispheres are shown in Figs. 4–8, as described below.

For M1, the time-course traces shown in Fig. 3 represent the average activity of 2340 voxels (V1) and 97 voxels (LGN) from 24 stimulus presentations; while for M2, the traces were generated from 19 stimulus presentations, averaging over 1404 voxels (V1) and 56 voxels (LGN). Note that a negative

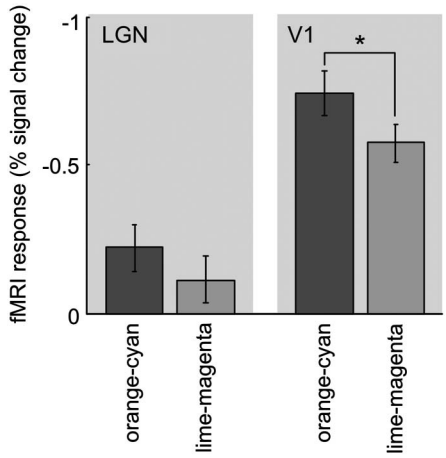

Fig. 4. Average LGN and V1 fMRI responses to orange–cyan and lime–magenta, across both fMRI experiments and both monkeys. Error bars show 95% confidence intervals. V1, $p = 0.02$ (t-test); LGN, $p = 0.27$ (t-test).

MION signal corresponds to an increase in the conventional BOLD fMRI signal. To facilitate a comparison with BOLD, the y axis in all the time-course traces presented in Fig. 3 (and Fig. 5) have been inverted: an upward deflection corresponds to a decrease in MION signal and an increase in neural activity. In all the time-course traces shown in Fig. 3 (for both LGN and V1), there are eight deflections, each corresponding to a stimulus block during which a grating was presented (see Fig. 1B). Between each block of grating stimulation, during presentation of the uniform neutral gray block, the neural response returned to baseline.

In the present analysis, we focus on the response to stimulus blocks during which the animals were shown orange–cyan gratings or lime–magenta gratings. For fMRI Experiment 1 these occurred during the sixth and eighth stimulus blocks (indicated in the time-course traces of Fig. 3 by gray shading). As described in Section 1, these colors were carefully chosen to elicit the same spatiotemporally averaged activity of the presumed LGN chromatic channels and are defined by the intermediate axes in the DKL color space. The LGN traces (top-left panels in Figs. 3A and 3B) are noisier than the V1 traces (bottom-left panels in Figs. 3A and 3B), which is not surprising given that the LGN is buried deep in the brain, relatively far away from the MR coils, and it consists of many fewer voxels. Despite this, the LGN shows clear deflections in signal response that correspond to the various stimulus blocks, showing that fMRI can be used to extract meaningful signals from the LGN. The V1 time-course trace is less noisy than the LGN trace and, for both M1 (Fig. 3A) and M2 (Fig. 3B), shows a higher peak during the orange–cyan block than during the lime–magenta block. The responses are quantified in the bar plots shown in the left panels of Fig. 3 (see Subsection 2.E).

The LGN responses to orange–cyan and lime–magenta for both experiments in the two animals were statistically indistinguishable (top bar plots in Figs. 3A and 3B; t-test $p = 0.14$, M1, Experiment 1; $p = 0.58$, M2, Experiment 1;$p = 0.31$, M1, Experiment 2; and $p = 0.81$, M2, Experiment 2). The V1 responses, on the other hand, were significantly different: the response to orange–cyan blocks was higher (bottom bar plots in Figs. 3A and 3B). This was true for both animals, in both fMRI experiments and for both hemispheres (t-test $p = 0.01$, M1, Experiment 1; $p = 0.0003$, M1, Experiment 2;

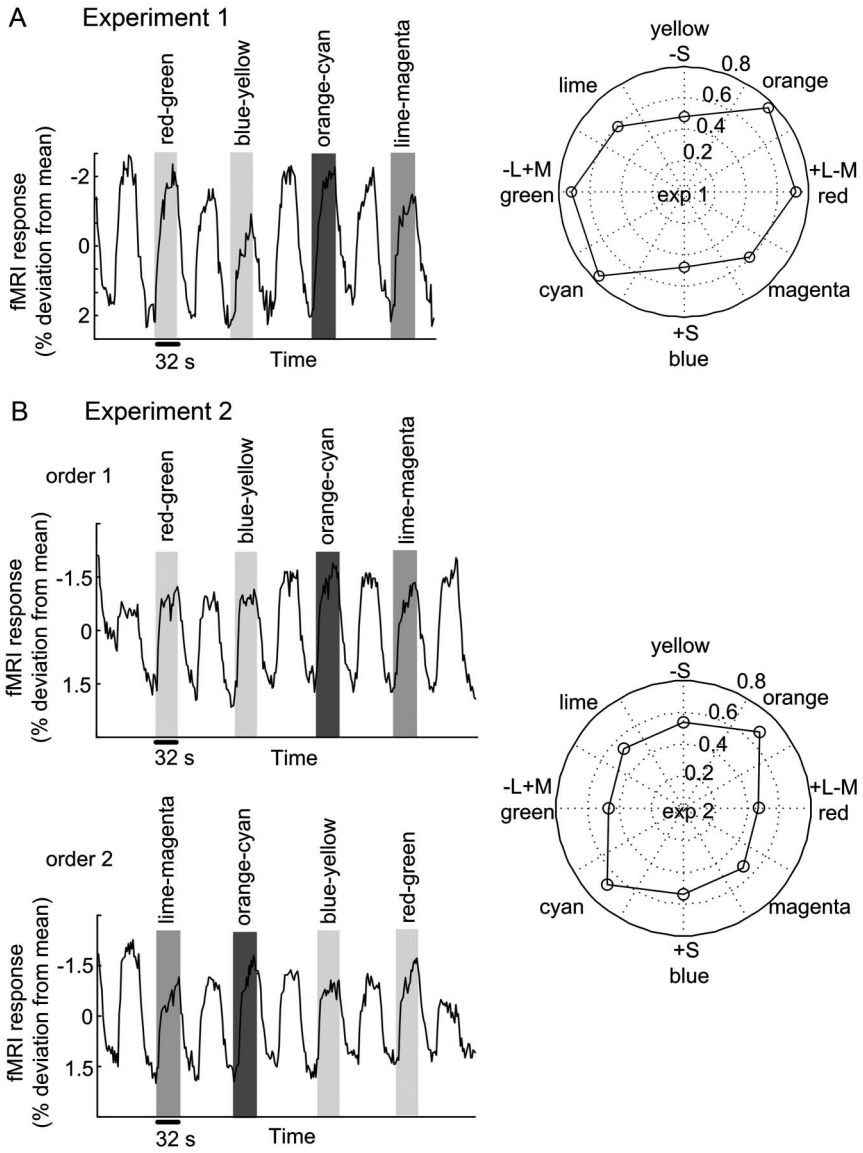

Fig. 5. Mean fMRI signal changes in V1 show elongation along the orange–cyan axis. Left panels show the percentage deviation (calculation described in Fig. 3, left panel) of the mean fMRI time course within V1 (both hemispheres) averaged across animals for each experiment ($n = 43$ stimulus presentations for Experiment 1 and $n = 41$ stimulus presentations for Experiment 2). Right panels show the absolute value of mean fMRI percent signal change (see Subsection 2.E) of V1 to the four colored blocks, which correspond to the four DKL chromatic axes depicted in Fig. 1. Distance from the origin in the polar plots indicates the absolute magnitude of the percent signal change calculated as in the bar plots shown in Fig. 3. A. Results of Experiment 1. B. Results of Experiment 2, which was conducted with two orders consisting of different temporal sequences of colored blocks (see Fig. 1).

and $p = 0.0015$, M2, Experiment 2), with the exception of the left hemisphere of M2, where the trend was consistent but not significant (t-test, $p = 0.1$). The subtle discrepancy between the two animals may be attributed to the smaller number of voxels comprising V1 in M2 (see Table 3).

To test whether the results from the individual experiments and individual hemispheres are representative, we determined the average response during the orange–cyan block and during the lime–magenta from both monkeys (all four hemispheres) and both experiments. Consistent with the analysis of the single experiments and single hemispheres shown in Fig. 3, the grand average showed that V1 had a greater magnitude fMRI response to orange–cyan than lime–magenta ($p = 0.02$), while the LGN did not ($p = 0.27$) (Fig. 4).

Although the LGN showed no statistically significant difference between the response magnitude to orange–cyan and lime–magenta, we observe a trend in the bar plots: as for V1, the response magnitude for orange–cyan was generally higher than that for lime–magenta. This was true in all conditions except for one LGN of one monkey in one experiment (the left LGN of M1 during Experiment 2) and is also reflected in the grand average (Fig. 4).

The relatively higher response to orange–cyan over lime–magenta can also be appreciated in the left panels of Fig. 5, which show the average time course of the response for each experiment (Experiment 1, Fig. 5A; Experiment 2, Fig. 5B), averaging the data from both hemispheres of both animals. The deflection of the trace during the orange–cyan blocks is higher than the deflection of the trace during the lime–magenta blocks, for both experiments (t-test $p = 0.0002$, Experiment 1; t-test $p = 0.002$, Experiment 2 averaging data from both orders).

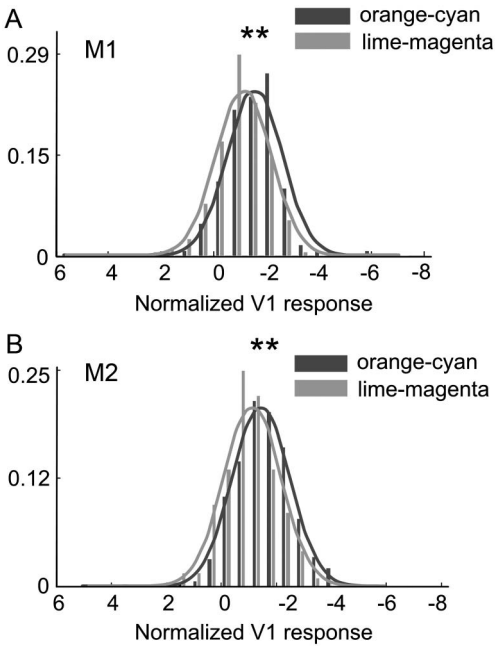

Fig. 6. Histograms of fMRI responses in V1 during orange–cyan and lime–magenta stimulation, combining responses from two recording sessions (Experiment 1 and Experiment 2) for each animal. Each count in the histogram represents the response of the entire V1 ROI during a given sample (one 2 s TR) during stimulus presentation; to avoid confounds attributed to the hemodynamic delay, only samples 7 to16 of each stimulus block were used in the analysis. A total of 370 samples were included for M1, and 470 samples for M2. Increasingly negative MION signals are plotted to the right to facilitate comparison with conventional BOLD responses. A. Response histograms for M1. B. Response histograms for M2. In both animals, the distribution of responses was more negative (corresponding to *higher* neural activity with MION) to orange–cyan than to lime–magenta (t-test, M1, $p = 2.2 \times 10^{-9}$; M2, $p = 0.004$).

The two experiments involved different temporal sequences of stimulus blocks (see Fig. 1B), which enabled us to evaluate whether the difference in response magnitude to the different color conditions is simply a function of the time during the scan when the color appears (as might be the case for a neural adaptation effect). But switching the order of the colored blocks did not affect the result: responses to orange–cyan were higher than to lime–magenta when orange–cyan appeared first (t-test $p = 8 \times 10^{-5}$, combining Experiment 1 and order 1 of Experiment 2) and also when it appeared second (t-test $p = 0.002$, Experiment 2 order 2). Therefore the difference in response magnitude between the intermediate color conditions cannot be attributed to some form of selective adaptation during the stimulus presentation but rather to the color that comprised the stimulus.

The right panels of Fig. 5 show polar plots in which the distance from the center of the plot corresponds to the magnitude (absolute value) of the fMRI response (percent signal change, as described in Subsection 2.E) to each color, and the angle corresponds to color of the stimulus as shown in the DKL color space given in Fig. 1. The polar plots are necessarily symmetric since the stimuli were heterochromatic gratings: the response assigned to "orange" is equivalent to the response to "cyan" as both were determined by the response to the orange–cyan heterochromatic grating (similarly for the other color pairs). The shape of the polar plot is elongated along the orange–cyan axis in Experiment 1 and Experiment

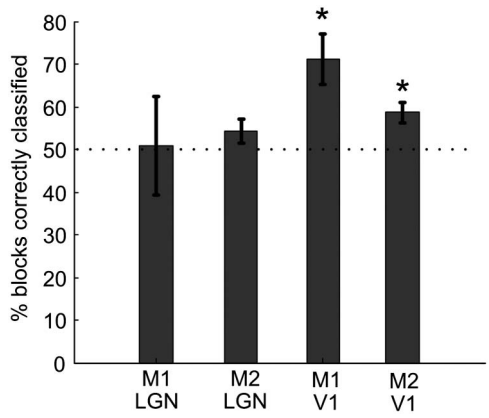

Fig. 7. Single-trial orange–cyan versus lime–magenta classification performance, by brain region, for univariate classification conducted on the basis of the voxel-averaged signal in each area, averaged over both hemispheres and two recording sessions in each of two monkeys (i.e., $n = 8$ data sets for each area). Each bar represents the mean percent of stimulus blocks that were correctly classified; error bars denote the standard error. The dashed line represents chance performance (50% correct). The asterisk indicates a $p < 0.05$ of achieving that classification performance by chance (unpaired t-test).

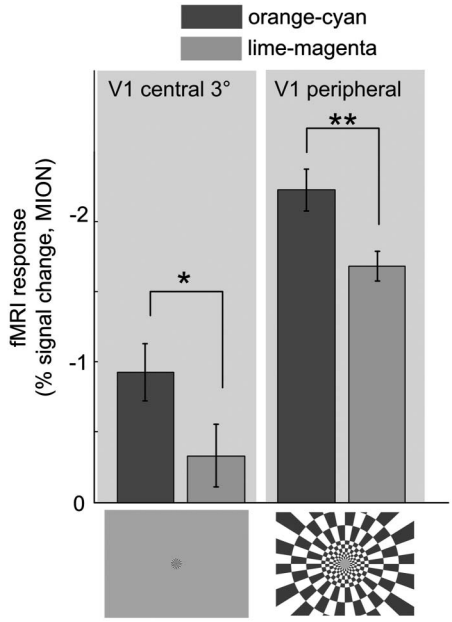

Fig. 8. Both central and peripheral V1 show larger fMRI responses to orange–cyan than lime–magenta. Central and peripheral representations were determined in an experiment during which a block of flickering checker dartboards (1 Hz) restricted to the central 3° of the visual field was alternated with a block of flickering checker dartboards restricted to peripheral regions outside of this central region. Higher functional activation elicited during the 3° stimulus was used to define the central 3° representation. Magnitude of fMRI responses to lime–magenta and orange–cyan were evaluated in both the central ROI and the peripheral ROI. Bar plots show the mean fMRI percent signal change (see Subsection 2.E) averaged across both animals, both hemispheres, and both experiments (1 and 2) ($n = 84$ stimulus presentations), with error bars representing one standard error ($p = 0.05$ for the central 3° and $p = 0.005$ for the peripheral). See Table 3 for voxel and presentation numbers.

2, again showing that V1 had a stronger response to orange–cyan over lime–magenta.

As described in Subsection 2.C, for both experiments the orange–cyan and lime–magenta stimuli were matched in cone contrast, although for Experiment 1 the ratio of $L-M$ cone contrast of the $L-M$ stimulus (red–green) to the S contrast of the S stimulus (blue–yellow) was higher than for Experiment 2 (see Table 2). The polar plots show a relative elongation along the $L-M$ (horizontal) axis in Experiment 1 compared to Experiment 2, which is likely attributed to this discrepancy between the two stimulus conditions. Note that the relatively stronger response to the orange–cyan colors over the lime–magenta colors is preserved despite these differences. In addition, we note that, for both experiments, the relative response to the $L-M$ cardinal axis is considerably stronger than the response to the S cardinal axis: even though the S cone contrast of the blue–yellow stimulus was about 4× as strong as the $L-M$ cone contrast of the red–green stimulus, the response to the red–green stimulus was larger (Experiment 1) or only slightly smaller (Experiment 2) than the response to the blue–yellow stimulus.

To enable a closer comparison with the results of Goddard *et al.* [3], in Fig. 6 we show histograms of the fMRI responses of V1 in the two monkeys during orange–cyan and lime–magenta stimulation, combining responses from Experiment 1 and Experiment 2. Each count in the histogram represents the response of all V1 voxels during a given sample (one TR). As elsewhere, we only analyzed responses during the latter two thirds of each stimulus block, corresponding to the seventh through sixteenth TR of each block. Figure 6A shows the response histograms for M1; Fig. 6B shows the response histograms for M2. The more negative MION signals (indicative of stronger responses) are plotted to the right of "0" in the histograms. For both animals, the best-fit curve representing the response to orange–cyan is shifted to the right relative to the curve representing the response to lime–magenta (t-test M1, $p = 2\times10^{-9}$; M2, $p = 6\times10^{-4}$).

B. Classification Analysis

We applied a classification algorithm in an attempt to predict which of the two intermediate color-axis stimuli were presented on individual blocks, on the basis of the functional signals from that block. The percent of blocks correctly classified as orange–cyan or lime–magenta by the algorithm provides a lower bound on the information about these stimuli available in real time from the neural signals in each ROI (V1 or LGN), as described in Subsection 2.F. Figure 7 shows univariate classification results pooled across hemispheres and imaging sessions in the two animals. The average LGN performance does not differ significantly from chance, but the average V1 performance is significant in both animals ($p < 0.05$, t-test). These results support the conclusion that differences in mean V1 signal amplitude between the two stimuli are available for informing perceptual discriminations.

We also conducted a spatial pattern classification analysis on both pooled data and on data obtained from individual hemispheres for each experiment (analysis not shown). This analysis failed to reveal more information as compared to that revealed by the univariate mean signal classification. The one exception was the left hemisphere in M2, in which the pattern classification (66% correct) was significantly above chance by permutation test in one session (95% confidence level) (data not shown).

C. Central versus Peripheral Stimulation

To determine whether the stronger response to orange–cyan over lime–magenta was present throughout the visual field, we determined the voxels of V1 representing the central 3° of the visual field and those representing peripheral regions from 3° to 20.5° eccentric in the horizontal direction and 16.5° in the vertical direction (the monitor display was 41° × 31°, and the fixation point was centered in the display). These ROIs were generated using the results from a separate set of experiments conducted in the same animals (see Subsection 2.D). Figure 8 shows the magnitude of the responses to the orange–cyan blocks and the lime–magenta blocks for the central ROI (left bar plots) and the peripheral ROI (right bar plots). For both ROIs, the orange–cyan response is stronger than the lime–magenta response (central 3°, $p = 0.05$; peripheral, $p = 0.005$).

Figure 8 also shows that the representation of the peripheral visual field had a higher response than the representation of the central 3° to both orange–cyan and lime–magenta. This may be attributed to a better match between the spatial frequency of the stimulus and the receptive-field size of peripheral neurons. The stimulus had a fixed, relatively low, spatial frequency across the visual field, yet the size of receptive fields of V1 neurons scales across the visual field—neurons representing the fovea have smaller receptive fields than those representing the periphery—so the stimulus would only have been of optimal spatial frequency for a restricted region of V1, likely outside the central 3°.

D. Single-Unit Analysis

The two-dimensional spatial and temporal organization of the cone inputs to double-opponent cells in V1 of macaque monkeys has been characterized [20,21]. Curiously the results show a consistent pattern: rather than a uniform distribution of relative cone activations that would predict a wide range of color preferences among double-opponent cells, most of these cells showed L cone activation pitted against a combination of M *and* S input. This result was originally described by Conway [20] and has since been confirmed by several groups [21,23–26]. More recently this pattern has also been seen in the S-OFF cells of the LGN [24,27,28]. Receptive fields from six double-opponent cells are shown in Fig. 9A; each plot shows the receptive field of each cone type mapped using sparse-noise cone-isolating stimuli and reverse correlation (see Subsection 2.G). In these plots, red depicts increased activation, and blue depicts suppression. In general, regions of each cell's receptive field that were excited by L cones were suppressed by M and S cones, while regions that were excited by M cones were excited by S cones and suppressed by L cones.

We quantified the inputs of the sample of cone-opponent cells described in [21] in which the responses to all three cone inputs were determined; the results are plotted in the DKL color space defined by the cardinal chromatic mechanisms (Fig. 9B). Most of the cone-opponent V1 cells fall in quadrants I and III, showing a correlation between the $L-M$ signals and the S signals ($p < 0.0001$; $r^2 = 0.25$); this distribution is consistent with the pattern described for the example cells

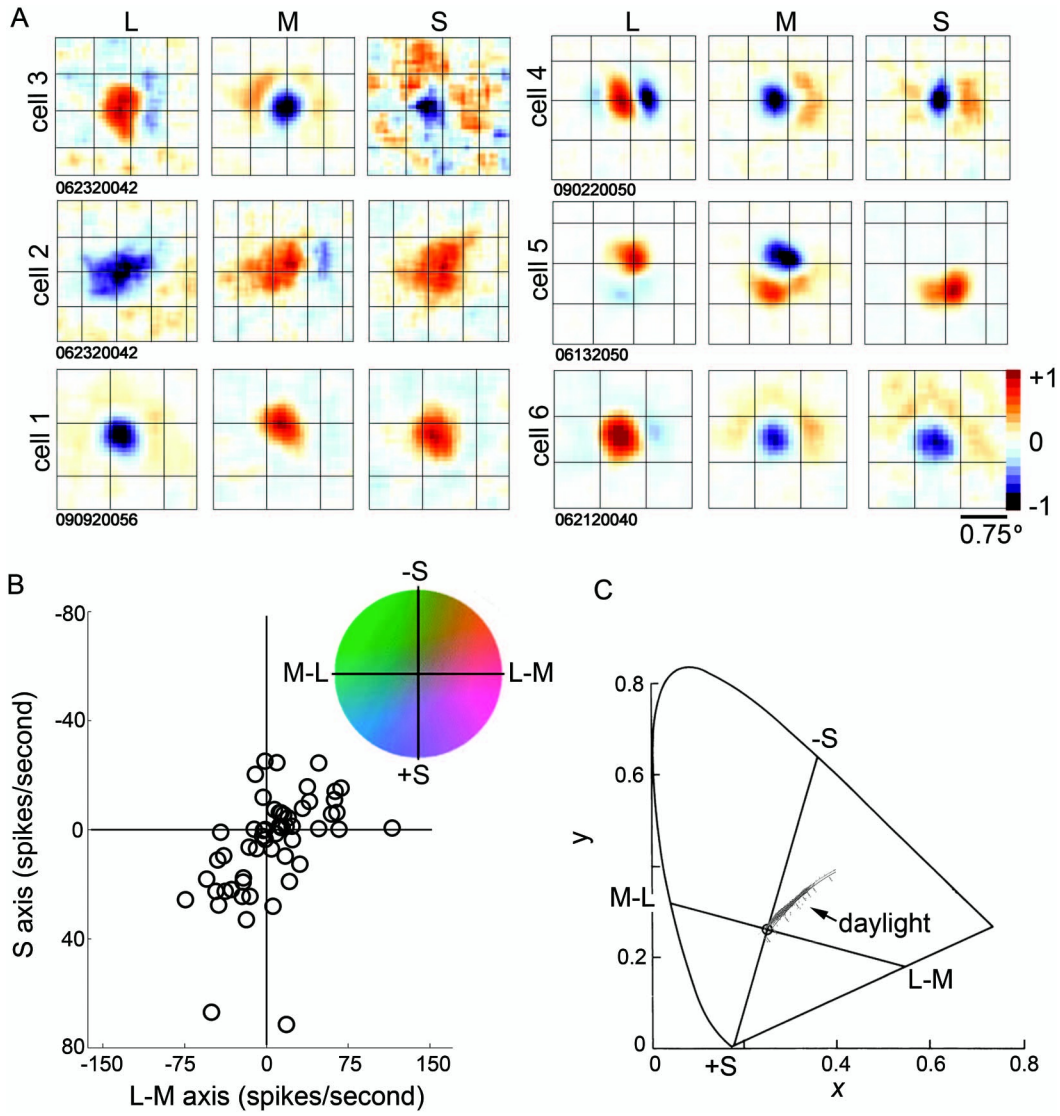

Fig. 9. The combination of cone inputs to cone-opponent cells in macaque V1 is predicted by the color of daylight. A. Each row shows for a single cell the spatial receptive-field response, at the peak time-to-response, to selective modulation of each cone class by itself. Receptive fields were in the near parafovea (~5°). The panels for cells 4–6 are reproduced from Conway and Livingstone [21]. B. Receptive-field center responses of the population of recorded cone-opponent cells ($N = 57$) plotted in cardinal chromatic coordinates; the receptive-field center was defined as the receptive-field subregion with the largest magnitude response. L minus M values were significantly negatively correlated with S values ($p < 0.0001$; $r^2 = 0.25$). For each cell we measured the response to six cone-isolating stimuli. These stimuli resulted in a selective increase or decrease in the activity of a single cone type. To determine each cone's response, the responses to stimuli that decreased the cone's activity were subtracted from the response to stimuli that increased the cone's activity. The values plotted on the x axis ($L - M$) were determined by subtracting the M-cone response from the L-cone response. Inset shows the DKL color space. C. The standard 1931 CIE color diagram showing the daylight axis (left) and a standard color space defined in cardinal retinal chromatic coordinates (right).

in Fig. 9A. The alignment of S inputs with M inputs is surprising: one might have predicted that, if $L - M$ opponent neurons received any S-cone input at all, it would align with the L input to account for the reddish quality of short-wave light [29]. Instead the combination of cone inputs is predicted by the daylight axis, shown in Fig. 9C projected onto the CIE color diagram. That the S stimulus aligns with that of the M stimulus (and not the L stimulus) cannot be attributed to a luminance artifact of some kind that might pair S with M, since the M and L stimuli have the same luminance sign.

4. DISCUSSION

We used fMRI to measure macaque LGN and V1 color-tuning responses to chromatic stimulation defined by the DKL color space; in addition, we analyzed the responses to cone-isolating stimuli of single cone-opponent neurons recorded extracellularly in macaque V1. Results from both fMRI and single-unit electrophysiology showed that V1 responds more strongly to orange–cyan intermediate colors than to lime–magenta intermediate colors. As we describe below, this tuning bias may represent an adaptation to daylight: V1, and especially the double-opponent cells, may function to extract spatial information from the color boundaries that are correlated with scene-structure cues, such as shadows lit by ambient blue sky and surfaces illuminated by sunshine. If true, these results raise the curious possibility that double-opponent cells have as much (or more) to do with perception of spatial information as they do with color appearance. This

might be surprising to some who consider spatial information to depend largely on color-blind luminance channels (which, the argument goes, is why scene structure is vivid in a black-and-white movie).

For the fMRI experiments, we focused our analysis on the responses to colors modulated along the two intermediate axes, which have been described as lime–magenta and orange–cyan [3]. These two heterochromatic stimuli would theoretically elicit the same combined response from the canonical subcortical (LGN) $L-M$ and S channels [3]. We found that stimuli modulated along the orange–cyan axis evoked larger fMRI responses in V1 than the responses evoked by stimuli modulated along the lime–magenta axis, whereas responses in LGN were statistically indistinguishable for the two stimuli—a difference in response in V1 to stimulation of the two intermediate axes has been interpreted as showing that V1 recombines the chromatic signals from the two canonical subcortical channels of the LGN [3]. Our experiments do not rule this out, although as described below, we may have undersampled the LGN response, and the color bias seen in V1 may turn out to be inherited from the LGN. A classification analysis revealed that V1 signals from individual stimulus presentations were sufficient to discriminate between these two stimuli at significantly better-than-chance performance. For the single-unit experiments, we evaluated the cone inputs of single cone-opponent cells. Consistent with the fMRI results, linear combinations of the responses to cone-isolating stimuli yielded stronger predicted responses to contrasts defined by the intermediate orange–cyan axis than by the lime–magenta axis (Fig. 9B); indeed the combination of cone inputs suggests these neurons are tuned along the orange–cyan axis. This result suggests the possibility that the stronger fMRI response in V1 to orange–cyan over lime–magenta is driven by a subset of V1 neurons, namely the cone-opponent cells, many of which are double opponent [20,21]. Both the single-cell results and the fMRI results confirm the presence of noncardinal color sensitivities in macaque V1, specifically the bias for orange–cyan among cone-opponent V1 cells [20,21,23–26].

The cone-opponent cells constitute only a relatively small subset of V1 cells (estimates vary from 3%–10% [20,21,23–26]). Can the color bias measured with fMRI be attributed to this small population of V1 cells? Possibly: as Heeger *et al.* have argued [30], relatively large fMRI responses can be driven by small changes in mean firing rate, which could be brought about by large modulations in the firing rate of a small population of neurons. The spatial frequency of the stimulus we used was relatively low (2.9 cycles/deg, drifting at 0.75 cycle/s), and would have been better matched to the relatively large receptive fields of V1 cone-opponent cells than it would have been to the majority of V1 neurons. Moreover, the chromatic stimuli we used lacked luminance contrast. Such equiluminant stimuli elicit robust responses from V1 cone-opponent cells but are not optimal for most V1 neurons, which fire vigorously to luminance contrast [31]. Taken together, the stimulus properties would be expected to elicit larger responses from cone-opponent cells than from most other neurons in V1. Thus, it would seem plausible that the fMRI bias for orange–cyan we measured was driven by cone-opponent neurons.

The fMRI results we obtained with monkeys are at odds with fMRI results in humans, which show a bias for lime–magenta over orange–cyan [3]. The discrepancy in the results of the two studies may point to a species difference, although these two species have often been assumed to be essentially homologous [32,33] and macaque monkeys have exactly the same cone photoreceptors as humans [34]. But the two species do not have identical preretinal filtering mechanisms [35], and these differences (especially of macular pigmentation) may introduce differences in the cone contrasts of stimuli presented to the cones. The results shown in Fig. 8 suggest that differences in prefiltering pigments are unlikely to be the cause of the color bias we observe since the bias is present following stimulation of the central visual field and stimulation of the peripheral visual field (Fig. 8), yet the retina corresponding to these two regions of visual field differs sharply in the amount of macular pigmentation. Besides potential species differences, there are methodological differences between the two studies. In the present report, the stimuli consisted of drifting vertical gratings that were equiluminant with the adapting background, whereas Goddard *et al.* [3] used stimuli, with circular organization (designed to match retinal receptive fields at varying eccentricities), that were not equiluminant. In addition, our study employed higher-resolution fMRI and MR contrast agents. But it is not clear to us how any of these differences could account for the difference in the results between the two studies.

A. LGN Responses

Our finding that LGN responses do not distinguish lime–magenta from orange–cyan contrasts is consistent with the long-established understanding that noncardinal mechanisms are absent or negligible in LGN [2,36]. Since the two intermediate color-axis stimuli were designed to activate the cardinal channels equally, one expects an equal LGN response to these two stimuli. On the other hand, our classifier results represent a lower bound on the stimulus-related information available in the neural signal in a given area, and we did observe a nonsignificant trend toward better-than-chance classifier performance in some recording sessions; this trend was consistent with one found for the magnitude of the responses in LGN—most of the bar plots in Fig. 3 show a higher response to orange–cyan than lime–magenta. That this trend did not reach significance may be a function of the small number of voxels in the LGN and the lower signal-to-noise of LGN fMRI responses (structures deep in the brain like the LGN will show lower fMRI SNR). Such a trend is consistent with the existence of LGN cells that show noncardinal tuning, specifically tuning comprising L signals pitted against a combination of $M+S$. As described above, such cells have recently been described in the LGN of macaques [28]. This leaves open the possibility that the noncardinal tuning seen in V1 (in both fMRI responses and cone-opponent single-unit recording responses) is inherited by V1 from the LGN.

B. Classification Analysis

Our classification analysis revealed noncardinal color contrast information available in V1 on single stimulus presentations, which could inform real-time perceptual representations. The pattern of classifier performance was consistent with the pattern of mean activations observed in the two animals, in that mean signals in LGN were indistinguishable by the classifier, while the single-block mean signal for V1 of both

monkeys significantly discriminated the orange–cyan from the lime–magenta stimuli. These performances mirror the pattern of overlap between error bars on the mean response to each stimulus (Fig. 3). With the statistically significant exception of M2's left hemisphere during one of two imaging sessions, in general the classification performed on the basis of the spatial pattern of voxel activations did not perform as well as the univariate classification conducted on the basis of the mean signal in each area. This is another difference between our study and Goddard *et al.* [3]: Goddard *et al.* report improved stimulus predictions using pattern classification. This might be attributed to their more effective classification algorithm, but we found that a backpropagation algorithm with fivefold cross validation designed to avoid overfitting problems common with large-dimensional data sets still did not improve classification of our data. This suggests that our classification's performances are limited by the data rather than the algorithm, which could be resolved by obtaining a larger data set in the monkeys. Alternatively, the difference might be accounted for in terms of differences in voxel size or imaging sensitivity between the two studies. Resolution of this awaits a comprehensive study of the spatial scale of color representations in humans and macaques.

C. V1 Color-Tuning Bias and the Daylight Axis

The color-tuning bias we find in V1 corresponds more or less to the daylight axis. Figure 9C shows the standard CIE 1931 color-space plot, in which the location of the spectral colors is depicted along the margins of the horseshoe; spectral samples from daylight are also plotted (daylight inset adapted from Fig. 2 in [37]), along with the two cardinal chromatic axes [2]. Under viewing conditions adapted to the color at the center of the CIE plot (neutral), at the intersection of the cardinal axes, the daylight axis progresses along colors that oppose L signals against $M + S$ signals, the same bias found in our fMRI results and found in the cone inputs of V1 cone-opponent cells (Fig. 9B).

Most of the cone-opponent cells in our population of recorded cells had receptive fields that showed both spatial and chromatic (i.e., "double") opponency, a structure that has been thought to contribute to the neural mechanisms that discount the spectral bias of the illuminant and lead to color constancy [20,38,39]. The combination of cone inputs of this population suggests that these cells would respond to chromatic boundaries formed by the colors of daylight (e.g., orange–blue boundaries), which are most closely approximated by those of the (so-called) orange–cyan intermediate axis. Note that the color names assigned to the orange–cyan axis are not representative of the perception of most observers—the axis is better described as "yellowish–orange and blue." An analysis of natural scenes shows that chromatic contrasts formed by the colors corresponding to the daylight axis are surprisingly common, even when sky is discounted [40]. Our results therefore suggest that V1 is adapted specifically to the diurnal chromatic conditions under which the visual system evolved.

But what function might sensitivity to orange–blue boundaries serve? Under natural daylight, objects are not illuminated uniformly. Because the sun is a single source of illumination, it will cast shadows that will be illuminated by diffuse ambient blue skylight, which reflect relatively higher power in the shorter wavelengths compared to sun-illuminated surfaces. Thus orange–blue boundaries could represent a meaningful cue to scene structure since they would indicate shadows and allow a representation of shape from shading. Indeed, the powerful role of color to inform scene structure is evident in many impressionist paintings. A notable example is Claude Monet's *Wheatstacks (End of Summer)*, painted in 1890–1891 (The Art Institute of Chicago). The chromatic bias of V1 further suggests that orange–blue contrasts should be more salient than other chromatic pairings, which has recently been demonstrated for human observers [41] and may account for the ubiquity of the orange–blue palette in movie advertisements [42]. Interestingly, observers report that contrasts associated with the daylight axis in natural scenes are most pleasing [43].

The physiological results presented here are compatible with human psychophysical data showing a greater contribution of adaptable mechanisms tuned to orange–cyan than to lime–magenta [44]. Additionally, the results are not incompatible with earlier reports showing that humans have higher thresholds to colors along the cardinal blue–yellow (S) axis [45]. In fact, the fMRI results reflect this observation: the responses to colors modulated along the S cardinal axis were smaller (Fig. 5A) or only slightly larger (Fig. 5B) than the responses to colors modulated along the $L - M$ cardinal axis even though the cone contrast of the S stimulus was substantially higher than the cone contrast of the $L - M$ stimulus (see Table 2). But our results do seem to be at odds with other findings, namely psychophysical results in humans showing that orange–cyan contrasts are less salient than lime–magenta contrasts in visual search tasks [46] and still other results showing that human discrimination thresholds are lowest along an axis closer to the lime–magenta axis than to the orange–cyan axis [47]. Coupled with the observation that a circle from a uniform color space plotted in DKL appears stretched along the orange–cyan axis, such observations would seem to suggest that adaptation to the natural world has brought about *less* sensitivity to those colors of highest contrast in nature, specifically colors along the daylight axis [48]. It remains unclear how to reconcile this paradox. One possibility is that the single-unit responses, which could conceivably drive the monkey fMRI results we observe (as discussed above), may be implicated in extracting spatial information like shape from shadows from color signals, rather than simply mediating color experience.

ACKNOWLEDGMENTS

This research was carried out in part at the Athinoula A. Martinos Center for Biomedical Imaging at the Massachusetts General Hospital, using resources provided by the Center for Functional Neuroimaging Technologies, P41RR14075, a P41 Regional Resource supported by the Biomedical Technology Program of the National Center for Research Resources (NCRR), National Institutes of Health. This work also involved the use of instrumentation supported by the NCRR Shared Instrumentation Grant Program and/or High-End Instrumentation Grant Program, specifically grant number S10RR021110. B. R. C. was supported by the Whitehall Foundation, the National Science Foundation, the Radcliffe Institute for Advanced Study at Harvard University, and Wellesley College. M. C. W. was supported by Wellesley College and the National

Science Foundation. Thorsten Hansen wrote the calibration program. Sebastian Moeller, Doris Tsao, and Joe Mandeville helped with the fMRI analysis programs. Larry Wald and Azma Mareyam provided the four-channel RF coil. Eric Erzinger and Josh Mcreedy designed and built the animal chair. Thanks to Bruce Fischl and Doug N. Greve for technical assistance with the FreeSurfer software. We are grateful to Mike Webster, Qasim Zaidi, Fred Kingdom, Kathy Mullen, Cleo Stoughton, Galina Gagin, Jeff Beck, Gabriel Kreiman, Jed Singer, and Alexander Rehding for useful discussions. We thank David Hubel, Margaret Livingstone, John Maunsell, Richard Born, and John Assad for their support.

†These authors contributed equally to this work.

REFERENCES

1. J. Krauskopf, D. R. Williams, and D. W. Heeley, "Cardinal directions of color space," Vis. Res. **22**, 1123–1131 (1982).
2. A. M. Derrington, J. Krauskopf, and P. Lennie, "Chromatic mechanisms in lateral geniculate nucleus of macaque," J. Physiol. **357**, 241–265 (1984).
3. E. Goddard, D. J. Mannion, J. S. McDonald, S. G. Solomon, and C. W. Clifford, "Combination of subcortical color channels in human visual cortex," J. Vision **10**(5):25, 1–17 (2010).
4. D. I. MacLeod and R. M. Boynton, "Chromaticity diagram showing cone excitation by stimuli of equal luminance," J. Opt. Soc. Am. **69**, 1183–1186 (1979).
5. B. R. Conway, S. Chatterjee, G. D. Field, G. D. Horwitz, E. N. Johnson, K. Koida, and K. Mancuso, "Advances in color science: from retina to behavior," J. Neurosci. **30**, 14955–14963 (2010).
6. R. T. Eskew, Jr., "Higher order color mechanisms: a critical review," Vis. Res. **49**, 2686–2704 (2009).
7. T. Hansen, Department of General and Experimental Psychology, Justus Liebig University Giessen, Otto-Behaghel-Strasse 10 F1, Giessen 35394 (personal communication, 2011).
8. Q. Zaidi, Graduate Center for Vision Research, State University of New York, College of Optometry, 33 West 42nd Street, New York, New York 10036 (personal communication, 2011).
9. D. B. Judd, "Report of U. S. secretariat committee on colorimetry and artificial daylight," in Vol. 1 of *Proceedings of the Twelfth Session of the CIE* (Bureau Central de la CIE, 1951), p. 11.
10. G. Wyszecki and W. S. Stiles, *Color Science: Concepts and Methods, Quantitative Data and Formulae* (Wiley, 1982).
11. T. Hansen, M. Giesel, and K. R. Gegenfurtner, "Chromatic discrimination of natural objects," J. Vision **8**(1):2, 1–19 (2008).
12. B. R. Conway and D. Y. Tsao, "Color architecture in alert macaque cortex revealed by fMRI," Cereb. Cortex **16**, 1604–1613 (2005).
13. V. C. Smith and J. Pokorny, "Spectral sensitivity of the foveal cone photopigments between 400 and 500 nm," Vis. Res. **15**, 161–171 (1975).
14. G. Paxinos, Huang X-F, and A. W. Toga, *The Rhesus Monkey Brain In Stereotaxic Coordinates* (Academic, 2000).
15. R. W. Cox and J. S. Hyde, "Software tools for analysis and visualization of fMRI data," NMR Biomed. **10**, 171–178 (1997).
16. B. R. Conway, S. Moeller, and D. Y. Tsao, "Specialized color modules in macaque extrastriate cortex," Neuron **56**, 560–573 (2007).
17. D. Y. Tsao, W. Vanduffel, Y. Sasaki, D. Fize, T. A. Knutsen, J. B. Mandeville, L. L. Wald, A. M. Dale, B. R. Rosen, D. C. Van Essen, M. S. Livingstone, G. A. Orban, and R. B. Tootell, "Stereopsis activates V3A and caudal intraparietal areas in macaques and humans," Neuron **39**, 555–568 (2003).
18. J. Winawer, H. Horiguchi, R. A. Sayres, K. Amano, and B. A. Wandell, "Mapping hV4 and ventral occipital cortex: the venous eclipse," J. Vision **10**(5):1, 1–22 (2010).
19. G. J. Brouwer and D. J. Heeger, "Decoding and reconstructing color from responses in human visual cortex," J. Neurosci. **29**, 13992–14003 (2009).
20. B. R. Conway, "Spatial structure of cone inputs to color cells in alert macaque primary visual cortex (V-1)," J. Neurosci. **21**, 2768–2783 (2001).
21. B. R. Conway and M. S. Livingstone, "Spatial and temporal properties of cone signals in alert macaque primary visual cortex," J. Neurosci. **26**, 10826–10846 (2006).
22. A. Stockman and L. T. Sharpe, "The spectral sensitivities of the middle- and long-wavelength-sensitive cones derived from measurements in observers of known genotype," Vis. Res. **40**, 1711–1737 (2000).
23. B. R. Conway, D. H. Hubel, and M. S. Livingstone, "Color contrast in macaque V1," Cereb. Cortex **12**, 915–925 (2002).
24. S. G. Solomon and P. Lennie, "Chromatic gain controls in visual cortical neurons," J. Neurosci. **25**, 4779–4792 (2005).
25. T. Wachtler, T. J. Sejnowski, and T. D. Albright, "Representation of color stimuli in awake macaque primary visual cortex," Neuron **37**, 681–691 (2003).
26. G. D. Horwitz, E. J. Chichilnisky, and T. D. Albright, "Cone inputs to simple and complex cells in V1 of awake macaque," J. Neurophysiol. **97**, 3070–3081 (2007).
27. S. G. Solomon and P. Lennie, "The machinery of colour vision," Nat. Rev. Neurosci. **8**, 276–286 (2007).
28. C. Tailby, S. G. Solomon, and P. Lennie, "Functional asymmetries in visual pathways carrying *S*-cone signals in macaque," J. Neurosci. **28**, 4078–4087 (2008).
29. C. R. Ingling, Jr., "The spectral sensitivity of the opponent-color channels," Vis. Res. **17**, 1083–1089 (1977).
30. D. J. Heeger, A. C. Huk, W. S. Geisler, and D. G. Albrecht, "Spikes versus BOLD: what does neuroimaging tell us about neuronal activity?" Nat. Neurosci. **3**, 631–633 (2000).
31. D. H. Hubel and T. N. Wiesel, "Receptive fields and functional architecture of monkey striate cortex," J. Physiol. **195**, 215–243 (1968).
32. B. R. Conway, "Color vision, cones, and color-coding in the cortex," Neuroscientist **15**, 274–290 (2009).
33. R. L. De Valois, H. C. Morgan, M. C. Polson, W. R. Mead, and E. M. Hull, "Psychophysical studies of monkey vision. I. Macaque luminosity and color vision tests," Vis. Res. **14**, 53–67 (1974).
34. D. A. Baylor, B. J. Nunn, and J. L. Schnapf, "Spectral sensitivity of cones of the monkey *Macaca fascicularis*," J. Physiol. **390**, 145–160 (1987).
35. D. M. Snodderly, J. D. Auran, and F. C. Delori, "The macular pigment. II. Spatial distribution in primate retinas," Investig. Ophthalmol. Vis. Sci. **25**, 674–685 (1984).
36. H. Sun, H. E. Smithson, Q. Zaidi, and B. B. Lee, "Specificity of cone inputs to macaque retinal ganglion cells," J. Neurophysiol. **95**, 837–849 (2005).
37. J. Hernandez-Andres, J. Romero, J. L. Nieves, and R. L. Lee, Jr., "Color and spectral analysis of daylight in southern Europe," J. Opt. Soc. Am. A **18**, 1325–1335 (2001).
38. N. W. Daw, "Goldfish retina: organization for simultaneous color contrast," Science **158**, 942–944 (1967).
39. A. Hurlbert and K. Wolf, "Color contrast: a contributory mechanism to color constancy," Prog. Brain Res. **144**, 147–160 (2004).
40. M. A. Webster and J. D. Mollon, "Adaptation and the color statistics of natural images," Vis. Res. **37**, 3283–3298 (1997).
41. D. Bimler, "Flicker between equal-luminance colors examined with multidimensional scaling," J. Opt. Soc. Am. A **27**, 523–531 (2010).
42. P. Sciretta, "Orange/blue contrast in movie posters," 2009, http://ohnotheydidnt.livejournal.com/41879586.html.
43. I. Juricevic, L. Land, A. Wilkins, and M. A. Webster, "Visual discomfort and natural image statistics," Perception **39**, 884–899 (2010).
44. J. Krauskopf and K. Gegenfurtner, "Color discrimination and adaptation," Vis. Res. **32**, 2165–2175 (1992).
45. A. L. Nagy, R. T. Eskew, Jr., and R. M. Boynton, "Analysis of color-matching ellipses in a cone-excitation space," J. Opt. Soc. Am. A **4**, 756–768 (1987).
46. K. C. McDermott, G. Malkoc, J. B. Mulligan, and M. A. Webster, "Adaptation and visual salience," J. Vision **10**(13):17, 1–32 (2010).
47. M. V. Danilova and J. D. Mollon, "Parafoveal color discrimination: a chromaticity locus of enhanced discrimination," J. Vision **10**(1):4, 1–9 (2010).
48. M. A. Webster, "Calibrating color vision," Curr. Biol. **19**, R150–R152 (2009).